Open Access

Catalysis Research

LIDSEN Publishing Inc.

Original Research

Methanol Synthesis Catalyst Waste as the Principal Component of New Sustainable Cementless Concrete

Vsévolod Mymrin[1, *], Reinaldo H. G. Alarcon [1], Marilia A. Guidolin [1], Kirill Alekseev [1], Rogerio J. Hultmann [2], Walderson Klitzke [1], Karina Q. Carvalho[1], Fernando H. Passig [1], Charles W.I. Haminiuk [2], Rodrigo E. Catai [1]

1. Academic Department of Civil Engineering, Federal University of Technology - Parana, str. Deputado Heitor Alencar Furtado, 5000, Campus Curitiba, 81280-340, CIC, Paraná, Brazil; E-Mails: seva6219@gmail.com; rhg727@gmail.com; maguidolin@utfpr.edu.br; ale-kirill@yandex.ru; rjhfilho@hotmail.com; wklitzke@gmail.com; karinae@gmail.com; fhpassig@utfpr.edu.br; catai@utfpr.edu.br
2. Academic Department of Science and Environmental Technology, Federal University of Technology - Parana, str. Deputado Heitor Alencar Furtado, 5000, Campus Curitiba, 81280-340, CIC, Paraná, Brazil; E-Mail: haminiuk@utfpr.edu.br

* **Correspondence:** Vsévolod Mymrin; E-Mail: seva6219@gmail.com

Academic Editor: Pankaj Kumar Parhi

Special Issue: Catalysis for Energy and Environmental Applications

Catalysis Research
2023, volume 3, issue 1
doi:10.21926/cr.2301009

Received: December 08, 2022
Accepted: February 09, 2023
Published: February 27, 2023

Abstract

Methanol synthesis catalyst (MSC) waste was applied as the principal component (till 70 wt.%) of sustainable ceramics in composites with bauxite processing waste (RM), and waste foundry sand (FS). The results of the initial components' chemical interaction studies by a complex of methods (XRD, SEM/EDS/mapping, AAS and LAMMA) during heating demonstrated the synthesis of amorphous glasslike new formation, their filling of pores and compaction of the ceramic's structure. In this case, a strong chemical and mechanical binding of all heavy metals and other hazardous elements of the initial industrial waste occurs with their transfer to an

insoluble in an acidic environment. The materials with the highest MSC contents have the highest axial resistance values ill 25.98 MPa after firing at 1050°C.

Keywords
Spent methanol synthesis catalyst; bauxite processing waste; steelmaking slag; sustainable construction materials; environment protection

1. Introduction

Significant increase in the Globe atmosphere temperature is responsible for many contemporary natural disasters like droughts, floods, devastating storms, giant fires and many human deaths. The main reason for the increase in the intensity of these tragic events is the contamination of the atmosphere with the dust of industrial and municipal waste annually released into dumps. Therefore, the urgent disposal of all industrial and municipal waste long-stored and newly produced, outgrows the problem of the survival or death of mankind in the following 300 years, scientifically calculated and predicted by S.W. Hawking. The results of an actual experimental study convincingly show the possibility of recycling at once three hazardous industrial wastes (methanol synthesis catalyst, red mud from bauxite processing and waste foundry sand) as valuable raw materials for the production of highly durable and environmentally friendly ceramic for civil construction instead of traditional natural materials such as clay and sand.

The total amount of waste generated in the European Union in 2010 was over 2.5 billion tons. The amount of waste from catalytic processes among them is small. However, their high content of heavy metals makes researchers develop the most diverse and reliable methods for their utilization.

According to McNaught and Wilkinson [1], a catalyst increases the speed of a reaction without changing Gibbs's total energy variation. In recent years, a large number of spent catalysts have been used in the potential production routes are composed of metals such as cobalt (ethanol production), iron-copper-rubidium in the Fischer-Tropsch process (olefins, gasoline, paraffin, and diesel), and copper-zinc-aluminum (methanol production) [2].

Therefore, intensive development of methods for using spent catalysts is being carried out worldwide, especially by isolating valuable heavy metals from them.

Worch and Dove [3] believe that catalytic chemical recycling or upcycling can alleviate numerous issues related to our current and future refuse and, in doing so, help pivot our materials economy from linearity to circularity. Luo, et al. [4] published an overview of the investigation of the relationship between structure and activity/selectivity on oxide-supported metal catalysts. Sutton et al. [5] published a paper containing an extensive literature review of the three main groups of catalysts (dolomite, alkali metals and nickel), which have been evaluated for the elimination of hydrocarbons of biomass gasification.

This study by Al-Sheeha, et al. [6] investigates the recovery of Mo, V, and Ni metals from the industrial spent hydro-processing catalyst, using various steps such as deoiling, drying, grinding, sieving, decoking, and treating with acid–base reactions in order to separate the various components of the spent catalyst. A spent equilibrium catalyst from the oil refinery company was partially replace sand and/or cement in concrete mixtures by Abdolpour, et al [7]. Applied catalysts

for the thermochemical recycling of plastic waste were analyzed by Huang, et al. [8]. Subramani and Gangwal [9] critically assesses various catalytic routes for converting syngas to higher alcohols, emphasizing ethanol. Kim, et al. [10] suggested methods to be highly applicable to upcycling Poly (ethylene terephthalate) waste PET. The leaching rate was enhanced by ultrasound, and large percentages (>95%) of all valuable metals (Mo, V, and Ni) present in the spent catalyst were extracted in a short time at a relatively low temperature (e.g., 60°C) by combined use of citric acid and ultrasound [11].

The second component of the initial mixtures of this study is red mud (RM), an industrial waste of bauxite ore beneficiation for aluminum production. The cumulative world stock of RM will be almost 4 billion tons by 2021 [12] with pH near 13. It is usually stored in factory dumps, polluting the environment and threatening the local population with a breakthrough in the walls of these dumps. The corner of an RM storage dam in Hungary (Turi, Pusztai, Nyari, 2013) [13] collapsed, and a wave of RM flooded the streets of a neighboring city, causing ten people to die (Carmo, Kamino, Junior, et al, 2017) [14]. The spill poured into the Danube and polluted 40 km^2 of land, contaminating the region's soil. RM's high heavy metal content (Cd, Pb, Cu, Cr, Zn) and high pH = 13 value caused by sodium oxide are two main reasons for its classification as hazardous industrial waste. A million cubic meters of the RM sludge of high alkalinity spilled from a reservoir at an alumina plants in Brazil [15, 16]. There were hundreds of victims, and the economic damage was several billion dollars.

Nevertheless, one of the problems of RM recycling is that customers do not accept products made from waste materials, especially in the case of bauxite tailings, which are hazardous waste materials [17]. The utilization of RM in road bases and asphalt mixtures was reviewed and future research priorities were pointed out by Lima and Thives [18]; Rychkov, et al. [19] intensified carbonate scandium leaching from bauxite red mud. (Liu, et al, 2014) [20] presented a completely different approach to RM recycling, where RM was treated as a valuable material for further extraction of metals and other elements. The main flaw of this approach was that it led to the generation of even more residues. RM was used as an adsorbent for enhancing ferricyanide removal [21]. Pontikes, et al. [22] replaced 20% ordinary Portland cement with calcined RM and hydrated lime without any loss of treated RM to foamed geopolymer.

Rai, et al. [23] comprehensively reviewed the disposal and neutralization methods of RM. They gave a detailed assessment of the work carried until now for the utilization of RM in the field of the building (geopolymers, clay material, cement, ceramics, fired and non-fired building materials, concrete industry), pollution control (in wastewater treatment, absorption and purification of acid waste gases), metal recovery (iron, titanium, aluminum, alkali, rare earth), coagulant, adsorbent, catalyst and in soil remediation.

A systematic review of the current literature on the use of RM and slag in the production of red mud-slag geopolymer was done by Qaidi et al. [24]. A deep investigation into the hydration mechanism of bauxite-calcination-method red mud-coal gangue-based cementitious materials was conducted by Zhang et al. [25]. They observed the microstructure of C-A-S-H gel as a main hydration product.

Results presented by Kurtoğlu, et al. [26] provide a guideline for modifying RM by HCl and H_2SO_4 at different molarities to tune its structural characteristics, potentially offering opportunities for its utilization as cost-effective and environmentally friendly solutions to various applications.

The results of Liu et al. [27] indicate that red mud calcined at 600°C has good cementitious activity due to the formation of poorly-crystallized Ca_2SiO_4. Recently, entropy-stabilized catalytic systems

have raised great concerns due to the urgent demand for functional materials aiming to realize chemical catalysis Gao, et al. [28].

Waste foundry sand (FS) is the liquid metal casting and molding residue. As a result of thermal shocks, the sand modifies its granulometric composition and, therefore, is discarded as industrial waste with a high content of heavy metals. The yearly production of FS is approximately 62.64 million metric tons (Singh K, Guleria, 2020) [29]. The ever-growing dumps of this type of waste also make it necessary to develop a wide range of methods for their disposal.

Martins, et al. [30] used FS as a partial substitute (10%, 20%, 30%, 40%) for natural sand in self-compacting concrete. Parashar, et al., 2020 [31], investigated the usability of waste foundry sand in self-compacting concrete (SCC) and reported that WFS is suitable up to a certain extent for the replacement of fine aggregate in concrete. It is possible to predict the mechanical properties of concrete containing FS using an artificial neural network assisted by a multi-objective multi-verse optimizer algorithm [32]. FS with 22% cement for paver production presented a compressive strength of 35 MPa in 28 days [33].

Dyer and Lima [34] experimentally proved that the microstructure, and physical and mechanical properties of hot mix asphalt with FS are similar to regular concrete asphalts. Yaghoubi studied waste foundry sand's bearing capacity and physical properties, et al. 2020 [35]; waste foundry sand was found suitable as an engineered fill and road embankment fill material. Mymrin, et al. [36] suggested foundry sand along with the addition of other industrial wastes for the sintering of environmentally-safe ceramics at 950-1050°C with samples' flexural strength values of up to 14 MPa. Coppio, et al. [37] experimentally proved that the concrete electrical resistivity changes according to the FS composition

This brief review of the scientific and technical literature on the methods of methanol synthesis catalyst waste, bauxite processing waste, and waste foundry sand shows the lack of information on the possibility of a complete replacement of traditional natural materials with these industrial wastes.

Therefore, the **objectives of the study** were**:**

1. To develop new composites of sustainable ceramic materials production only from three hazardous industrial wastes (methanol synthesis catalyst waste, bauxite processing waste, and waste foundry sand) without application of the traditional raw materials like clay, sand and similar;
2. To study the values of all physical, mechanical and ecological properties of the developed ceramics, which must comply with Brazilian technical and environmental norms;
3. To study the processes of developed materials' structure formation and the influence of each component on these processes to regulate the values of their properties.

2. Materials and Methods

Raw materials characterization.

2.1 Materials

Three types of industrial wastes-methanol synthesis catalyst (MSC), red mud (RM) from bauxite processing and waste foundry sand (WFS)-were used as the only raw materials components of the developed ceramics, completely replacing traditional raw materials (natural clay and sand).

The representative sample of MSC was obtained at the factory near Curitiba. The sample of RM was received from an aluminum factory in Sao Paulo after the extraction of $Al(OH)_3$ from bauxite processing. The sample of waste foundry sand was obtained in the steel plant of the company Gerdau, in Curitiba.

2.2 Methods

To study the raw materials and the developed composites' physicochemical processes of structure's formation, the following complex methods were applied: mechanical, physical and environmental properties of the raw materials and developed ceramics were carried out by particle size distribution by laser diffraction analysis in combination with sew method; chemical composition by X-ray fluorescence analysis (XRF); mineral composition by X-ray diffraction (XRD) with an automated database of minerals PDF-2; the chemical composition of new formations by the method of energy-spectrum spectroscopy (EDS) and isotope composition by laser micro-mass analysis (LAMMA); morphological structure by scanning electron microscopy (SEM); solubility and leaching of metals-by atomic absorption analysis (AAA); the dispersion of the principal chemical elements in ceramics' new formations by mapping method.

The following studies were applied to investigate the mechanical and physical properties of the ceramics' test samples: flexural resistance strength, water resistance, water absorption, expansion and shrinkage.

2.3 Calculations

The water resistance coefficient (C_{WR}) was determined based on the ratio:

$$C_{WR} = \frac{R_{SAT}}{R_D} \quad (1)$$

where R_{SAT} is the axial compressive strength of saturated TSs after total immersion in water for 24 hours; and R_D is the axial compressive strength of the specimen oven-dried at 100°C for 24 hours.

Water absorption values were calculated in accordance with by the equation:

$$WA = \left[\frac{(Mh - Md)}{Md}\right] \cdot 100 \quad (2)$$

where, WA-the absorption of water by the test sample (%), Ms-mass of the sample after drying in oven at a temperature of 110°C for 24 hours (g) Mh-mass of the humid test sample after immersion in water at room temperature for 24 hours (g). At this moment, I, Vsevolod Mymrin, consciously assure that for the manuscript /insert title/ the following is fulfilled: 1) This material is the authors' original work, which has not been previously published elsewhere. 2) The paper is not currently being considered for publication elsewhere. 3) The paper reflects the author's research and analysis truthfully and completely. 4) The paper properly credits the meaningful contributions of co-authors and co-researchers. 5) The results are appropriately placed in prior and existing research context. 6) All sources used are properly disclosed (correct citation). Copying of text must be indicated as such by using quotation marks and giving proper references. 7) All authors have been personally and actively involved in substantial work leading to the paper, and will take public responsibility for

its content. The violation of the Ethical Statement rules may result in severe consequences. To verify originality, your article may be checked by the originality detection software authenticate. I agree with the above statements and declare that this submission follows the policies of solid-state Ionics as outlined in the Guide for Authors and in the Ethical Statement.

3. Results and Discussion

The research results are presented in three sections: 1. Raw materials characterization; 2. Mechanical and physical properties of the developed materials; 3. Physicochemical processes of their structure's formation, explaining the reasons for these properties obtaining.

3.1 Raw Materials Characterization

3.1.1 Particle Size Distribution of the Raw Materials

All raw materials were crushed on a jaw crusher, dried till the constant weight at 100°C, milled in a ball mill and sieved on a sieve 1.14 mm. After grinding the main part of MSC particles (66.39%) have a size between 0.15-0.29 mm and the maximum number (86.37%) of the smallest particles between 0- and 0.29-mm. RM has 39.33% of the coarsest particles between 0.60 and 1.19-mm. FS exhibited a more uniform size composition, with an 81.45% particle content ranging from 0.30 to 0.59 mm. Similar granulometric composition of RM was also described by Damayanti and Khareunissa (2011) [38]. The bulk density of MSC was 1.17 g/cm^3, RM-3.2 g/cm^3, and FS-2.65 g/cm^3.

The FS presented a minimum humidity level (of 1.52%) (Table 1), because it is a waste from high-temperature processes, unlike red mud, which had high (32.21%) humidity due to a chemical reaction with NaOH solution.

Table 1 Particle size distribution (wt.%), bulk density (g/cm^3) and humidity (wt.%) of the raw materials.

	Size (mm)	MSC	Red mud	Foundry sand
Grain size distribution	0-0.074	1.35	0.32	0.17
	0.075-0.149	17.63	1.08	1.54
	0.15-0.29	66.39	13.14	16.20
	0.3-0.59	14.63	46.13	81.45
	0.6-1.19	0	39.33	0.64
	≥ 1.2	0	0.00	0.00
Bulk density (g/cm^3)		1.73	3.16	2.65
Humidity (wt.%)		41.35	32.21	1.52

3.1.2 Chemical Composition of the Raw Materials

The chemical composition of the MSC determined by the RXF method (Table 2) mainly consists of copper oxide (58.23%), zinc oxide (24.00%), and aluminum oxide (6.05%). The principal oxides of RM are Fe_2O_3 (29.85%), Al_2O_3 (21.16%), SiO_2 (15.51%) and Na_2O (10.36%), and ignition loss (I.L. 16.24%), which coincides with many aluminum smelters in the world. In

particular, the red mud of the aluminum smelter plant in Tayan, West Kalimantan [38] of Indonesia has Fe_2O_3 (28.6%), Al_2O_3 (23.3%), SiO_2 (16.88%) and Na_2O (6.78%). The foundry sand mainly consisted of SiO_2 (88.2%), Fe_2O_3 (4.0%), SO_3 (2.0%), CaO (1.5%) and Al_2O_3 (2.3%). Some researchers (Oliveira and Holanda, 2004) [39] and Wendling, Douglas, Coleman (2009) [40] rather informed similar chemical compositions of ferrous slag.

Table 2 Chemical composition of the raw materials (by XRF method).

Oxides	Compositions, wt.%			Oxides	Compositions, wt.%		
	MSC	RM	FS		MSC	RM	FS
SiO_2	0.00	15.51	88.16	CaO	1.53	4.22	1.53
CuO	58.23	0.00	0.00	MgO	0.00	0.17	0.00
ZnO	24.00	<0.15	0.00	TiO_2	0.00	2.38	0.00
Al_2O_3	6.05	21.16	2.34	P_2O_5	0.00	0.00	0.00
SO_3	0.25	0.00	2.02	BaO	0.00	0.00	0.00
Fe_2O_3	0.11	29.85	4.04	Cr_2O_3	0.00	<0.10	0.26
Na_2O	0.00	10.36	0.00	I.L.	10.83	16.24	1.74
K_2O	0.12	0.26	0.00	Total	100.0	100.0	100.0

Note: I.L. – Ignition Loss.

The high content of the non-bonded chemical element in the liquid extract of acid solutions was detected by the AAS method. The results (Table 2) showed that leaching of all metals from flotation waste highly exceeded the demands of Brazilian standard sanitary norms NBR 10.004 [41]: Solid waste: As-in 5 times, Cr-2.3 times, Cd-9 times, Pb-6 times, Hg-22 times, Se-2 times.

High Na_2O content (10.3%) significantly reduced the melting point of the ceramics' composites. Foundry sand consisted mainly of SiO_2 (93.2%). The presence of 3.7% I.L. was most likely due toclogging with organic materials when preparing the molding form and when stored in industrial dumps.

Spent foundry sand essentially contained SiO_2-89.06%, and Al_2O_3-4.02%, with impurities of Fe_2O_3-1.06% and SO_3-1.03% and rather low C.L. = 4.15%. The study of the AAS method's leaching and solubility of metals from red mud showed (Table 3) a high content of all metals, including heavy metals, also far exceeding Brazilian standards [41].

Table 3 Leaching and solubility of metals from red mud and composition 6 after sintering at 1150°C.

Chem.	Leaching, mg/L				Solubility, mg/L			
elements	MSC	Comp.5	Comp.6	[41]	MSC	Comp.5	Comp.6	[41]
As	5.12	0.27	0.18	1.0	7.40	<0.001	<0.001	0.01
Cr total	11.29	0.86	1.26	5.0	18.53	0.02	0.01	0.05
Ba	79.13	0.86	1.22	70.0	82.15	0.02	0	0.7
Cd	4.35	0.09	0.13	0.5	9.22	0	0	0.005
Pb	6.19	0.10	0.15	1.0	8.06	<0.01	<0.01	0.01
Hg	2.17	0.12	0.05	0.1	3.11	<0.001	<0.001	0.001
Se	1.92	0.14	0.27	1.0	2.26	<0.001	<0.001	0.01

Al	2.16	0.11	0.19	*	5.13	0.11	0.04	0.2
Mn	3.55	0.14	0.08	*	5.21	0.07	0.02	0.1
Fe	23.47	0.43	0.73	*	29.16	0.1	0.04	0.3
Cu	7.72	0.07	0.04	*	8.28	0.49	0.25	2.0
Zn	6.38	0.04	0.08	*	7.45	0.76	0.54	5.0

A significantly more excess of hazardous chemical elements when comparing with the requirements of the same standards for the solubility of metals: Al-in 25 times, Mn-in 52 times, Fe-97 times, Cu-4 times, Zn-1.5, As-740, Cr-371, Ba 117, Cd-1844 times, Se-in 226 times.

3.1.3 Mineral Composition of the Raw Materials

The XRD pattern of MSC (Figure 1a) shows the presence of the crystalline minerals melaconite (CuO), zincite (ZnO) and berlinite ($AlPO_4$) with a rather high content of amorphous materials. The scale of the intensity of the peaks of crystalline structures of MSC almost reaches 1,500 counts per second (I cps), indicating a larger quantity of crystalline structures than the other two wastes. The highest of them belongs to melaconite and berlinite.

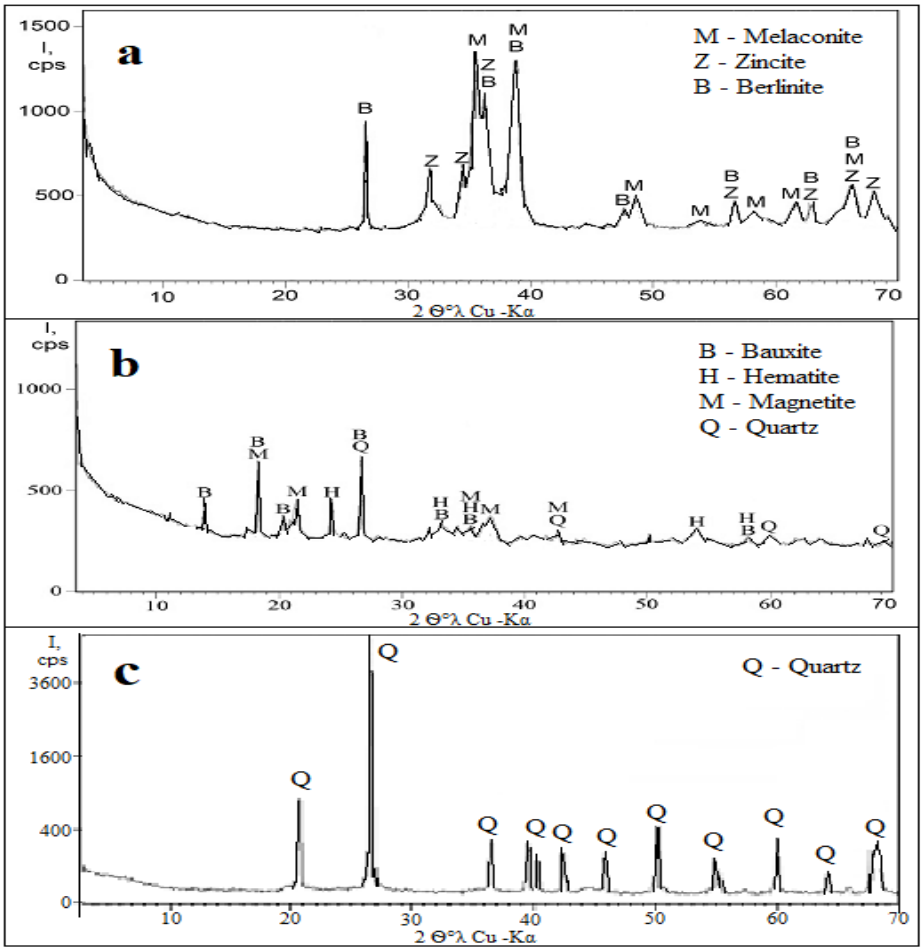

Figure 1 X-rays diffractogram patterns of the raw materials: **a**-waste of methanol synthesis catalyst, **b**-red mud, **c**-foundry sand.

The mineral composition of the bauxite treatment RM (Figure 1b) is presented by the rest of the untreated bauxite $Al_2O_3 \cdot xH_2O$, hematite Fe_2O_3 and magnetite Fe_3O_4 and a very small quantity of quartz SiO_2. Only two minerals' crystalline peaks at the angles of 2Θ° = 18° and 26.5° have intensities near 700 cps due to the coincidence of the two minerals' peaks; all other peaks barely exceed the x-ray background line. That means the approximal equality of crystalline and amorphous phase in RM, or even the predominance of the amorphous phase over the crystalline.

The diffractogram patterns of the FS (Figure 1c) demonstrate extremely low crystalline peaks (with I cps near 200-300 cps) and the biggest container the amorphous materials. Such a ratio of amorphous and crystalline phases should lower the melting point of materials; the low of potassium (63.6°C) and zinc (419.5°C) will also reduce the melting temperature of the initial mixtures. Conversely, a relatively high copper content (58.23%) in MSC with a sufficiently high melting point (1,084°C) can neutralize the effect of these elements.

3.1.4 Morphological Structure of the Raw Materials

The analysis of the MSC sample by SEM method (Figure 2a), in the magnifications at 5,000 times, presents cloudy conglomerates of irregularly shaped particles of different sizes from 1 to 4 μm with deep cracks, apparently due to grinding of the material. The RM sample (Figure 2b) at the same 5000 times magnification is represented by smaller particles from 1 to 2 μm.

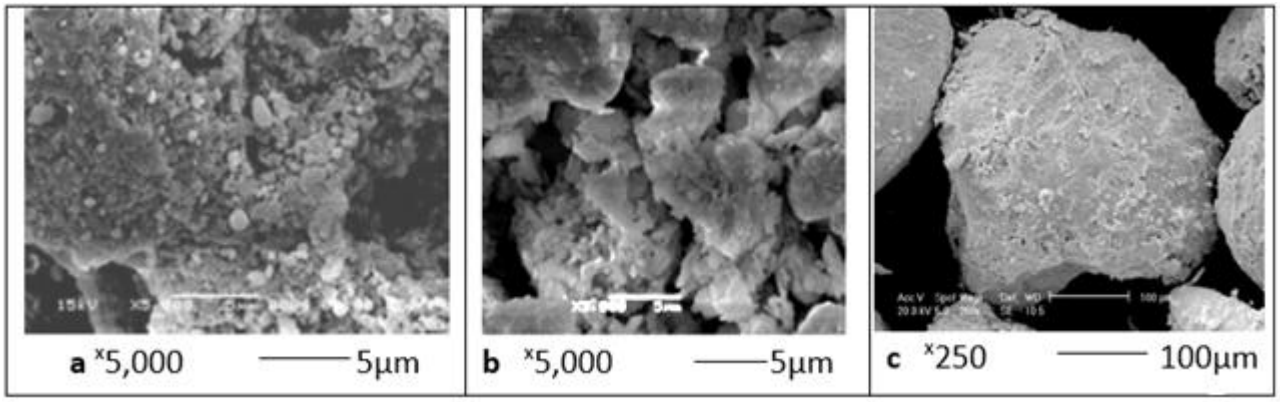

Figure 2 Morphological microstructures of the raw materials: **a**-waste of methanol synthesis catalyst, **b**-bauxite red mud, **c**-waste foundry sand.

These particles have mainly rounded shapes typical for amorphous materials and are divided by pores also of various shapes and sizes. The degree of aggregation of these particles is much lower than that of MSC.

The ferrous slag particles after milling are presented (Figure 2c) by the grains of 40-50 μm size, with a very dense monolithic structure.

3.2 Mechanical Properties of the Developed Ceramics

The values of flexural resistance, linear shrinkage, and water absorption of the compositions submitted to sintering at 900°C, 1000°C, 1050°C, 1100°C and 1150°C were measured and discussed.

3.2.1 Flexural Resistance of the Developed Ceramics

It is observed (Table 4) that the highest resistance (28.42 MPa) at all temperatures had ceramics 5 with the biggest (70%) of MSC, 30% RM and zero content of FS. The MSC substitution in the ceramics 5 by 10% red mud (ceramics 6) causes a strong decrease in the resistance of the ceramics at all temperatures; particularly, at 1050°C it was 23.76 MPa with the following beginning of excessive melting at 1100° and complete melting at 1150°C. The third place in the ceramic's strength values is occupied by ceramics four, with very high (60%) MSC content and beginning excessive melting between 1050°C and 1100°C.

Table 4 Flexural resistence of the developed ceramics after sintering at different T°C.

Compositions (wt.%)				Flexural resistence (MPa) after 0at T°C					
N°	MSC	RM	FS	900°	950°	1000°	1050°	1100°	1150°
1	0	90	10	2.14	2.94	3.40	3.98	5.12	6.79
2	0	80	20	1.83	2.11	2.64	3.44	4.28	6.90
3	50	0	50	1.11	3.38	7.62	9.72	10.23	4.65
4	60	0	40	1.62	4.20	8.92	17.34	11.03	Melt.
5	70	30	0	4.11	13.56	18.40	28.42	11.28	Melt.
6	60	40	0	0.93	8.11	15.22	23.76	9.38	Melt.
7	45	40	15	2.65	3.41	4.75	7.27	5.32	Melt.
8	50	30	20	2.90	7.52	11.35	6.17	Melt	Melt.
9	40	50	10	1.82	5.69	10.82	12.48	5.22	Melt.
10	30	55	15	2.17	4.93	7.85	11.69	14.23	5.26

Note: Melt. – means complete melting of the test samples.

Complete substitution of MSC by 80-90% of RM with 10–20% of FS in ceramics 1 and 2 leads to the lowest strength indices of all ceramics of the Table 3. These ceramics continued strengthening at 1150°, while all other ceramics were melted.

The substitution in ceramic 5 of 20% MSC by 20% of FS (ceramic 8) is accompanied by decreasing in the melting point of ceramics 8 between 1000°C to 1050°C with almost complete melting of these test samples at the following temperature of 1050°C.

All these facts indicate the principal positive influence of MSC on the flexural resistance of the developed ceramics.

Replacing 10% FS with an equal amount of MSC (compositions 3 and 4) causes an increase in sample strength from 9.72 to 17.34 MPa at 1050°C, followed by an accelerated onset of excessive melting of ceramic composition 4 at 1100°C.

The replacement of 30% FS in composition 3 by 30% RM in composition 8 causes an accelerated increase in the strength of ceramic sample 8. It reduces their melting point to the temperature range 1000°C–1050°C.

Replacing 15% MSC in composition 7 with RM in ceramic 10 leads to a significant increase in the strength of ceramics at all temperatures. An even greater increase in the strength of the samples occurs when replacing 40% RM (composition 1) with MSC (composition 9).

Flexural resistance values of all developed composites correspond to the maximum requirements of the Brazilian standards NBR 7170 [42] (2012) for ceramic blocks-class 15 = 1.5 < 2.5, class 25 = 2.5 < 4.5.

The standard deviation values of the flexural resistance from the obtained experimental data never exceeded 4% of the average means.

3.2.2 Linear Shrinkage of the Developed Ceramics

The values of the developed ceramics' linear shrinkage (LS) increased with increasing the sintering temperature (Table 5). The ceramics 1 and 2 with zero contents of MSC had less LS after sintering at all temperatures. Their insignificant compaction can explain this fact during firing ongoing thermochemical processes of the component's interaction, which determines their low resistance (1.83-6.90 MPa) at al sintering temperatures.

Table 5 Linear shrinkage of the developed ceramics after sintering at different temperatures.

Compositions (wt.%)				Linear shrinkage (%) after sintering at T°C					
N°	MSC	RM	FS	900°	950°	1000°	1050°	1100°	1150°
1	0	90	10	1.20	1.43	1.56	3.45	4.72	1.30
2	0	80	20	1.11	1.35	1.44	2.92	4.93	3.32
3	50	0	50	2.15	4.12	7.09	8.16	8.74	6.15
4	60	0	40	2.22	4.27	7.11	7.52	6.15	Melt.
5	70	30	0	6.70	12.58	13.22	14.03	10.32	Melt
6	60	40	0	5.55	10.09	12.25	13.39	11.44	Melt
7	45	40	15	3.26	4.80	7.67	9.46	9.15	Melt
8	50	30	20	3.03	4.25	7.84	8.73	Melt.	Melt
9	40	50	10	3.30	8.19	10.83	13.83	10.64	Melt
10	30	55	15	2.83	5.98	8.62	11.30	9.11	2.39

The ceramics 5 and 6, with zero FS content, had the maximum shrinkage values at all temperatures, confirming the role of FS particles as a skeletal additive. The chemical composition of MSC includes 58.2% of Cu with a melting point of 1080°C and 24% of Zn with a melting point of 420°C (total of 82.2%). During firing they produce a well-known alloy called brass with a melting point of 880°C-950°C, which depends on the percentage of these two metals. Exactly in this temperature range appeared an increase in the flexural resistance of ceramic samples 5 and 6 (Table 3) and their linear shrinkage by 2-3 times (Table 5). The resulting brass can serve as a bonding glue-like mass for 30-40% of the RM of the ceramics 5 and 6, but also as a flux for its melting.

Therefore, the ceramics 3 and 4 with maximum (50 and 40%) FS contents also had the minimum (after ceramics 1 and 2) shrinkage values also at all temperatures. Shrinkage values closest to composition 10 are observed for ceramics 7 with 15% content of FS.

The standard deviation values of the linear shrinkage were between 3-5%.

3.2.3 Water Absorption (W_{ABS}) of the Ceramics after Sintering

The study of changes in water absorption (Table 6) is of great interest, since this characteristic is an indirect indicator of changes in the open porosity of materials. The value of W_{ABS} steadily changes with increasing temperature of ceramics sintering due to the formation of gases during three processes: 1. burnout of the organics; 2. sulfur from an FS (2.0%) and MSC (0.3%, Table 2), 3. the exit of water from the crystalline structure of bauxite $Al_2O_3 \cdot xH_2O$ (Figure 2b). Rather high values of Ignition Loss (I.L., Table 2)-10.8% of MSC, 16.2% of RM and 1.7% of FS-confirmed the inevitability of these reactions which are reasons for pores' formation when firing ceramics. But there is still a fourth reason, most effective and difficult to calculate: 4. gases of the thermo-chemical interaction of the components' mixtures.

Table 6 Water Absorption (W_{ABS}) of the Developed Ceramics after Sintering.

Composition (wt.%)				Water absorption (%) after sintering at T°C				
N°	MSC	RM	FS	900°	1000°	1050°	1100°	1150°
1	0	90	10	21.68	19.11	20.61	14.52	7.05
2	0	80	20	23.07	21.68	19.40	13.66	6.43
3	50	0	50	19.84	16.38	11.78	7.57	4.11
4	60	0	40	17.53	15.57	10.24	7.03	Melt.
5	70	30	0	10.45	9.32	5.47	3.39	Melt.
6	60	40	0	11426	10.63	6.48	4.16	Melt.
7	45	40	15	12.39	11.00	9.43	5.00	Melt.
8	50	30	20	13.80	11.27	9.44	Melt.	Melt.
9	40	50	10	19.59	12.26	9.49	4.38	Melt.
10	30	55	15	20.12	11.47	7.65	6.44	Melt.

The highest values of W_{ABS} belonged to ceramics 1 and 2 with 90% and 80% RM of bauxite RM and 10-20% FS, which is the best explanation for such low characteristics of these two ceramics. Ceramics 5 and 6 had the lowest W_{ABS} values at all temperatures before the start of excess melting at 1050°C due to the maximal (70% and 60%) of MSC contents.

The values of the standard deviation of water absorption of ceramics after sintering at all temperatures do not exceed 0.4%.

3.3 Physical-Chemical Processes of Structure Formation of the Developed Ceramics

To study the physical-chemical processes of structure formation of the ceramics, two compositions were selected-5 and 6; both of them demonstrate the best resistance (Table 4) before the beginning of the excessive melting, the highest linear shrinkage (Table 5) and the lowest water absorption (Table 6).

3.3.1 Mineralogical Composition of Ceramic 5 after Firing at Temperature 1050°C

Comparison of the XRD pattern of the ceramic 5 (Figure 3) with de XRD pattern of the raw materials (Figure 1) demonstrates the increase in the intensity of the main peaks from 1400 cps to 2100 cps, which indicates, the successful thermochemical destruction of the crystalline lattice of

bauxite and its low content in the flotation sludge. On the other hand, it indicates satisfactory conditions for the synthesis of a new mineral albite ($NaAlSi_3O_8$) with a more intense peak at 2Θ° = 39.2° during ceramic 5 sintering at 1050°C.

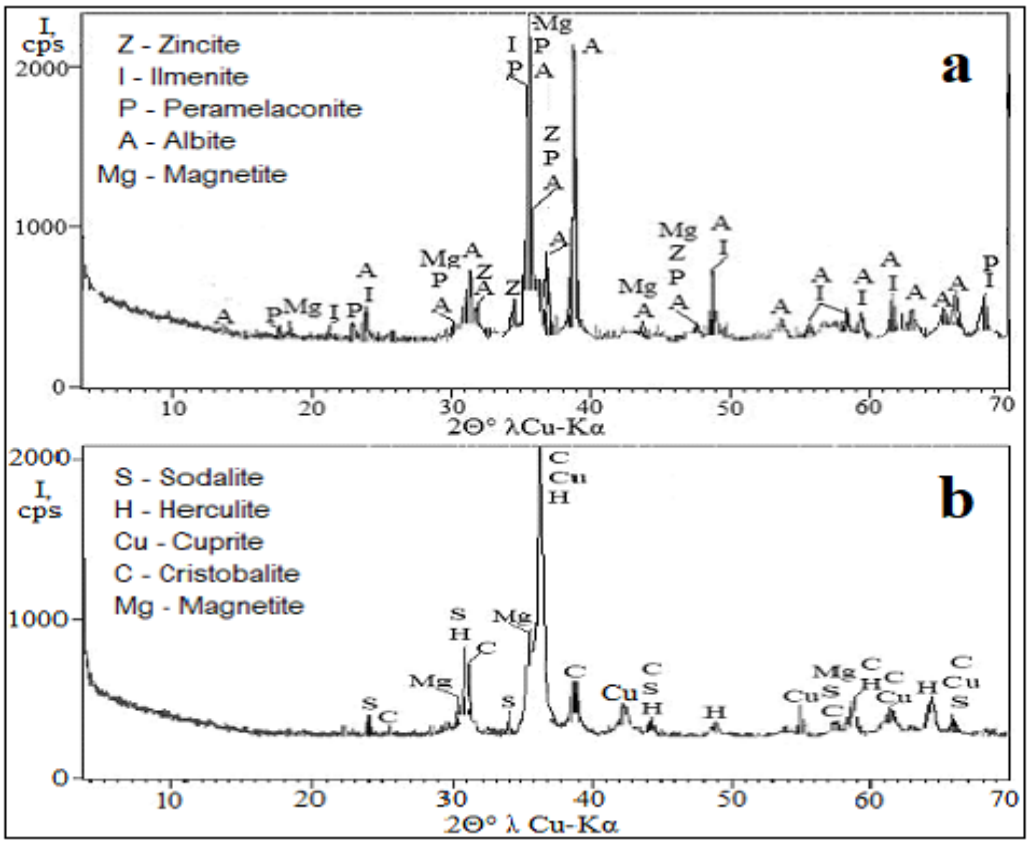

Figure 3 XRD patterns of the ceramics 5 (**a**) and 6 (**b**) after sintering at 1050°C.

Almost all initial minerals of the raw materials disappeared because of thermo-chemical destruction and synthesis of other new minerals, such as magnetite Fe_3O_4 due to the predominance of Fe_2O_3 (29.9%) in red mud; paramelaconite (Cu_4O_3) due to 58.2% CuO in MSC; zincite ZnO confirmed by 24.0% in MSC; albite ($NaAlSi_3O_8$) synthesized by the presence of Al in all components; small peaks of ilmenite $FeTiO_3$ because of the presence of TiO_2 (2.4%) in RM.

A small decrease in the vertical scale of peak intensity confirmed the common increase of amorphous phase in ceramics 6 compared to ceramics 5. It can be one of the reasons for ceramics' 6 higher flexural strengths (Table 4) at all temperatures before the beginning of excessive melting.

3.3.2 Morphological Structure of Ceramic 5 and 6 after Sintering at Temperature 1050°

The better density of the morphological structure of the ceramics 10 in comparison with the ceramics 9 and after sintering at 1050°C was confirmed using the SEM method (Figures 5a and b).

Less quantity of open and closed pores, cracks, and more completely molten particles in the structure of the ceramic sample 6 can explain these differences in the properties of the two materials. Practically all pores of the ceramics 6 are closed in contrary to many deep (black) pores of different configurations and sizes from 1 to 18 μm of the ceramics 5. On the surface of the ceramic sample 5, unbound particles or insufficiently fused particles are visible, which cannot increase the

solidity and strength of the structure, in contrast to the structure of ceramics 10 with a wave of completely molten material.

3.3.3 Microchemical Composition of the New Formations of the Ceramics 9 and 10 after Sintering at Temperature 1050°C

Results of EDS microchemical composition analyses of the new formations (Figure 4) of the ceramics 5 (points 1-3) and 10 (points 4-6) after sintering at a temperature of 1050°C (Table 7) showed a very high level of heterogeneity of all nearest points. Some of them differed in the set of chemical elements and their percentage ratio neither within the limits of each ceramic, nor in comparing these two ceramics.

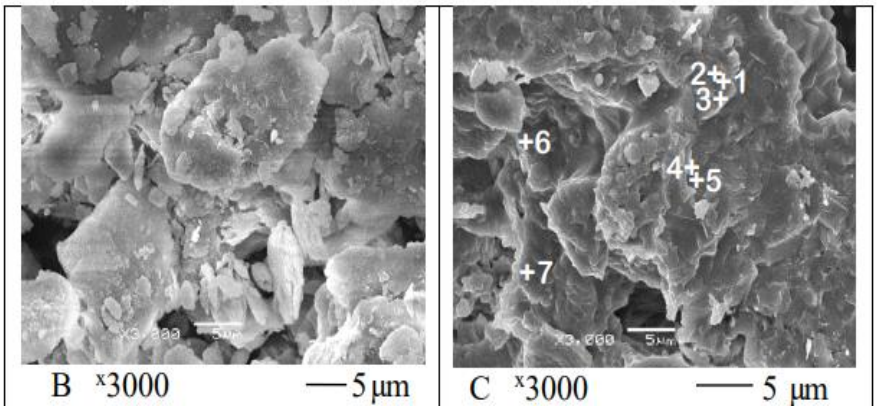

Figure 4 Morphological structure of the composites 5 (**a**) and 6 (**b**) sintered at 1050°C and points of EDS analyses.

Table 7 Microchemical composition of new formations of the ceramics 5 and 6 after sintering at temperature 1050°C by EDS method (Figures 4a and b).

Points	Content of chemical elements (wt.%) in the EDS points									
	Na	Al	Si	S	Ca	Ti	Fe	Cu	Zn	Total
1	7.22	12.46	13.39	0.62	0.83	0	5.84	44.21	15.43	100.0
2	0	1.03	0	0.85	0	0	1.11	89.26	0	100.0
3	17.28	0.86	11.10	0	11.32	0	1.17	26.09	32.18	100.0
4	15.63	1.12	2.03	4.19	0	0	0.53	72.35	4.15	100.0
5	0	0	12.53	8.74	20.01	0.53	0	8.45	49.56	100.0
6	0	20.33	6.17	0	3.04	1.07	18.28	10.52	40.59	100.0
7	9.18	18.21	12.90	4.63	1.25	1.22	15.97	6.45	30.19	100.0
Max.	17.28	20.33	13.39	8.70	0.01	1.67	18.28	89.26	51.94	
Min.	0	0	0	0	0	0	0	8.45	0	

These results well explained the complexity of the chemical composition of the initial mixture (Table 2) for the synthesis of new minerals with a perfect crystalline structure at 1050°C, confirmed by the XRD analysis (Figure 4). Therefore, all the maximum and minimum values of all nine chemical elements of Table 6 have differences from zero to 49.56% (Zn), or from 8.45% to 89.26% (Cu).

3.3.4 Isotopes' Composition of the Ceramics 5 after Sintering at Temperature 1050°C

The study of the nearest points of ceramics 9 after firing it at 1050°C by the laser micro-mass analyses (LAMMA) method (Figure 5) showed a large difference both in the atomic mass units (amu) of the isotopes and in their intensity (peak intensities). These results confirm both the results of the EDS (Figure 4 and Table 7), and the results of the XRD (Figure 4).

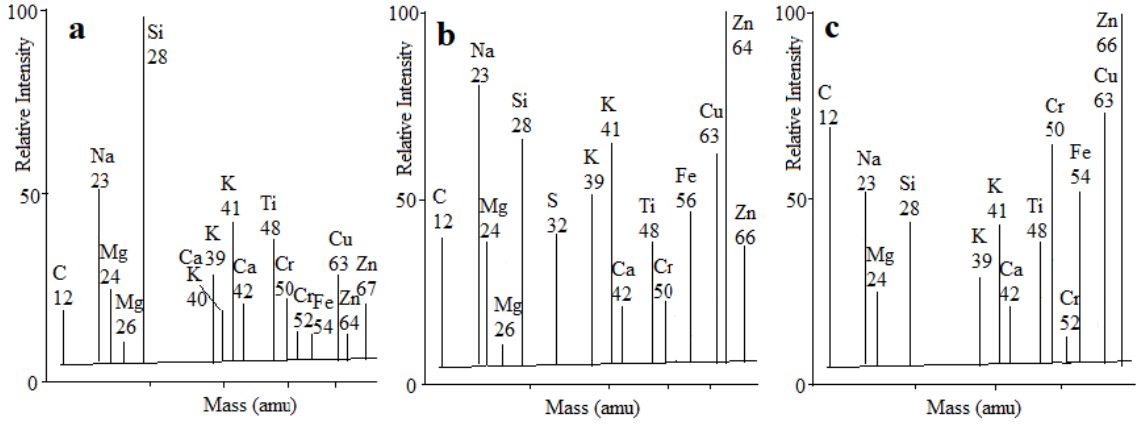

Figure 5 Isotopes' composition of the nearest points of the ceramics 5.

3.4 Mapping of Chemical Elements of the Ceramic 5 after Sintering at 1050°C

The method of mapping the chemical elements (Figure 6) on the scanning electron microscopy was used to study their distribution in a ceramic sample 5 after firing at 1050°C. This analysis made it possible to verify the great irregularity of their position for two possible reasons:

1. insufficient homogenization of the initial components before compaction and firing; 2. synthesis of microcrystals during the firing and cooling of the samples, which is confirmed by the results of the XRD (Figure 3).

The maximum distribution uniformity stands out for Ti, followed by Fe, Ca and Si the maximum unevenness had-Al, Na, Zn, Cu. But the general irregularity of the chemical element's distribution confirmed the predominant amorphism of the developed ceramic materials.

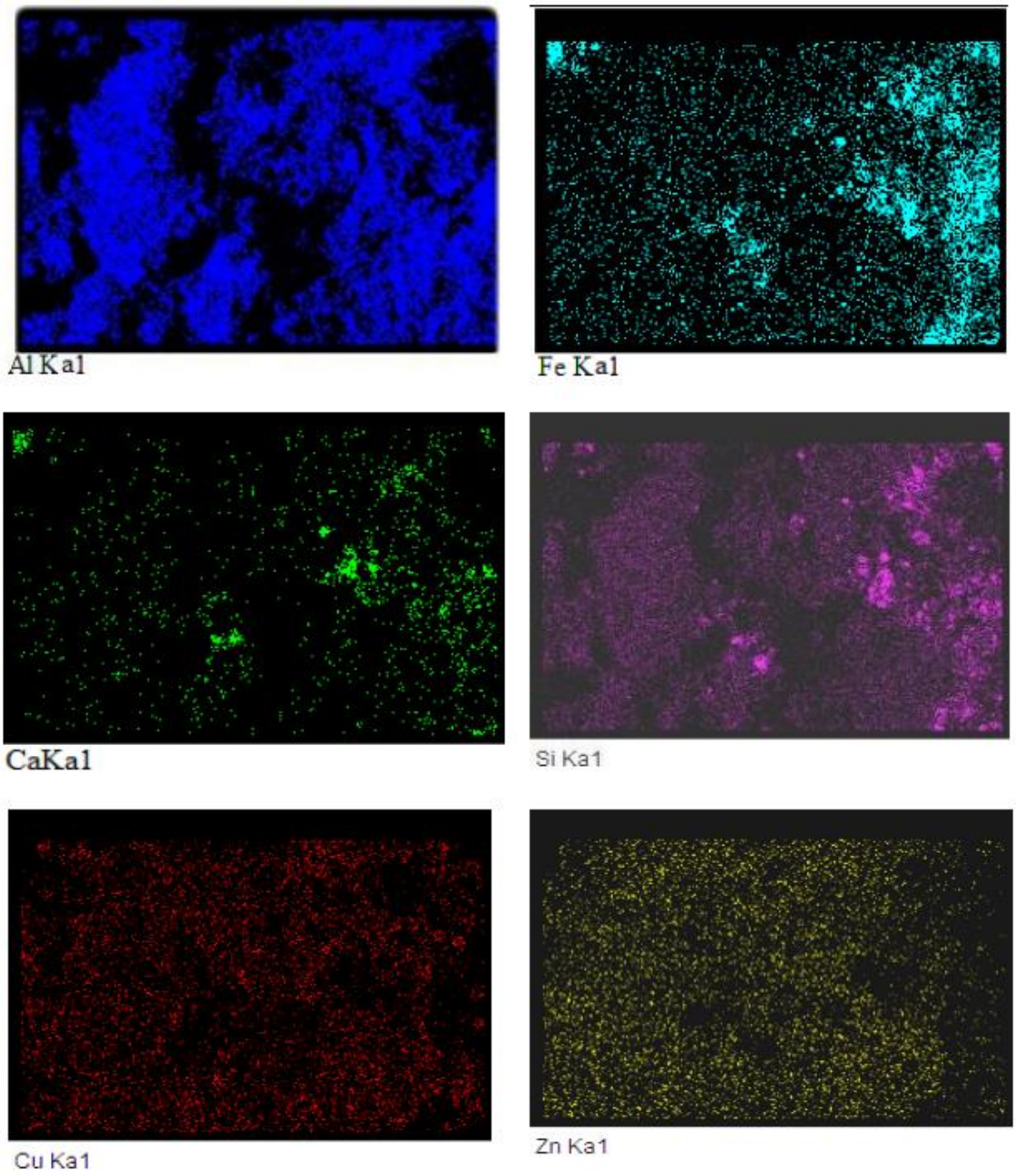

Figure 6 Mapping of principal chemical elements of the ceramic 5 after sintering at 1050°C.

3.5 Environmental Characteristics of the Ceramics 5 and 6 by AAS Method

3.5.1 Leaching and Solubility of the Developed Ceramics

Leaching and solubility tests from ceramics 9 and 10 in acid solutions allow us to evaluate the effect of thermo-chemical bonding of metals in the process of test samples' firing at 1050°C to prevent environmental pollution by the developed ceramics. The values of leaching and solubility are given (Table 2) in comparison with the sanitary standards NBR 10.004 [41] and the initial methanol synthesis catalyst (MSC) used as the most environmentally hazardous component of the ceramics. The leaching of all hazardous chemical elements (Table 2) from ceramics 9 in comparison with MSC decreased in 13 (Se and Cr) till 110 (Cu) times: solubility-in 17 times (Cu) till 4057 times

(Ba). Leaching values of the composition 10 decreased in 8 times (Cr and Se) and to 193 times (Cu); solubility values of the ceramics 10 decreased from 33 times (Cu) to 8218 times (Ba). This comparison confirmed strong chemical bonding (or mechanical capsulation) of all hazardous metals in practically insoluble new mainly amorphous glass-like formations of ceramics during their sintering at 1050°C. All obtained leaching and solubility values are significantly lower than permissible sanitary norms NBR 10.004 of Brazil [41].

3.5.2 Gas Emission Control Results during Ceramics Sintering (by AAS Method)

Samples of the heat gases were collected during ceramics' sintering at 1,275°C in the glass filter with a thickness of 0.45 μm. The separation of the solid particles deposited on the filter was performed by ultrasound (after three hours in an acidic medium) and determined by the AAS method (Table 8).

Table 8 Gas emission rates during the sintering of the developed ceramic.

Heavy metals	Contents, mg/Nsm³	NBR 10.004] [42], mg/Nm³
Cu	1.720	5.0
Cd	0.055	0.2
Pb	0.313	5.0
Cr	0.426	5.0
Ni	0.261	1.0

These results, along with leaching and solubility tests (Table 3), convincingly confirmed the robust bond of heavy metals in insoluble and non-volatile condition.

4. Economic Efficiencies of the Application of the Developed Materials

It is impossible to estimate the economic efficiency of using industrial wastes without information on the application in specific places with the local price of natural raw materials, distances and delivery prices, and many other data sources. Therefore, the calculation of economic efficiency was not included in the objectives of this study. Nevertheless, in common sense, free industrial wastes must be very cost-effective instead of relatively expensive natural. Also, considering that the tailings are materials that have already been extracted, crushed and processed (methanol synthesis catalyst, bauxite red mud), the real beneficiation costs for their reuse are significantly lower compared to the primary ores tailing that need to go through the entire mining beneficiation process, since processing represents about 40 to 60% of the total mineral processing cost.

5. Conclusions

1. It was confirmed that hazardous industrial waste used in this research as the raw materials-methanol synthesis catalyst (MSC), red sludge from bauxite processing (RM) and waste foundry sand (FS)–can be used as valuable raw materials for the production of ceramic materials instead of traditional natural raw materials like clay and sand.

2. The best mechanical and physical properties were obtained with two ceramic compositions: 1. 70wt.% MSC and 30% RM, and 2. 60% MSC and 40% RM. Their flexural resistance reached 28.42 and 23.76 MPa correspondingly after sintering at 1050°C, linear shrinkage till 14.03% and 13.39%, and water absorption–5.47% and 6.48%. These properties far exceeded the demands of Brazilian national norms for ceramics materials.

3. It was proved by the complex of XRD, SEM, EDS, LAMMA and chemical elements mapping methods that during the sintering of the ceramics at 1050°C the thermochemical dislocation of almost all minerals of the initial components and the synthesis of a small amount of new crystalline minerals occurred. However, the decisive role in the structure formation processes and properties of the developed ceramics is played by amorphous glassy formations, which fill the pores of the materials.

4. By the method of atomic absorption analysis of a liquid extract obtained in an acidic medium, it has been established that the developed ceramic firmly binds or reliably encapsulates all hazardous elements into an insoluble state. This allows them to use them as building materials. At the end of their service, their demolition waste can be used as crushed stone to produce new environmentally friendly construction materials. This allows the use of a large amount of hazardous industrial waste as a valuable raw material, improving the environment of the industrial region. At the same time, it becomes possible to reduce the destruction of unrecoverable natural ties by quarries of traditional natural building materials.

5. The calculation of the economic efficiency of the production of developed materials was not part of the purpose of this study, because each time it depends on many specific local parameters. But from common sense, using free raw materials (hazardous industrial waste) instead of costly natural building material is always much more profitable.

Acknowledgments

The authors bring their gratitude to the staff of Electron Microscopy Laboratory of the Federal University of Technology (UTFPR) and to the UFPR Laboratory of Minerals and Rocks for their technical assistance.

Author Contributions

Vsévolod Mymrin-author of the idea, developer of the plan of the experiments, participant of all stages of the research, corresponding author. Reinaldo H. G. Alarcon-test samples formation and atomic absorption and SEM analyses. Marilia A. Guidolin-test samples formation, SEM analyses. Kirill Alekseev-test samples formation, bibliography revision. Rogerio J. Hultmann-LAMMA analyses. Walderson Klitzke-samples sintering and gas emission control co-author of this manuscript. Karina Q. Carvalho-bibliographic studies, performer of all types of laboratories works. Fernando H. Passig-XRD analises. Charles W.I. Haminiuk-FRD and XRF analyses. Rodrigo E. Catai-bibliographic studies, performer of all types of laboratories experimental works, co-author of this manuscript.

Competing Interests

a. Funding not available.
b. We declare absence any conflicts of interest.

c. The raw/processed data required to reproduce these findings cannot be shared at this time due to legal or ethical reasons.
d. Code availability (software application or custom code) not applicable.
e. Ethics approval (include appropriate approvals or waivers) not applicable.
f. We show informed consent and provide assurances that participants' rights are protected.
g. All co-authors are consent for publication.

References

1. McNaught AD, Wilkinson A. IUPAC—Compendium of chemical terminology (the "Gold Book"). Oxford: Blackwell Scientific Publications; 1997.
2. Coutinho JP, Silva MC, Meneghetti SM, Leal E, de Melo Costa AC, de Freitas NL. Combustion synthesis of $ZnAl_2O_4$ catalyst using glycine as fuel for the esterification and transesterification of soybean oil: Influence the form of heating. Mater Sci Forum. 2012; 727-728: 1323-1328.
3. Worch JC, Dove AP. 100th anniversary of macromolecular science viewpoint: Toward catalytic chemical recycling of waste (and future) plastics. ACS Macro Lett. 2020; 9: 1494-1506.
4. Luo L, Hernandez R, Zhou X-D, Yan H. Heterogeneous catalysis at metal-oxide interfaces using in situ and operando spectroscopy: From nanoparticles to single-atom sites. Appl Catal A. 2021; 624: 118330.
5. Sutton D, Kelleher B, Ross JR. Review of literature on catalysts for biomass gasification. Fuel Process Technol. 2001; 73: 155-173.
6. Al-Sheeha H, Marafi M, Raghavan V, Rana MS. Recycling and recovery routes for spent hydroprocessing catalyst waste. Ind Eng Chem Res. 2013; 52: 12794-12801.
7. Abdolpour H, Niewiadomski P, Sadowski Ł. Recycling of steel fibres and spent equilibrium catalyst in ultra-high performance concrete: Literature review, research gaps, and future development. Constr Build Mater. 2021; 309: 125147.
8. Huang J, Veksha A, Chan WP, Giannis A, Lisak G. Chemical recycling of plastic waste for sustainable material management: A prospective review on catalysts and processes. Renew Sust Energ Rev. 2022; 154: 111866.
9. Subramani V, Gangwal SK. A review of recent literature to search for an efficient catalytic process for the conversion of syngas to ethanol. Energy Fuels. 2008; 22: 814-839.
10. Kim DH, Han DO, In Shim K, Kim JK, Pelton JG, Ryu MH, et al. One-pot chemo-bioprocess of PET depolymerization and recycling enabled by a biocompatible catalyst, betaine. ACS Catal. 2021; 11: 3996-4008.
11. Marafi M, Stanislaus A. Waste catalyst utilization: Extraction of valuable metals from spent hydroprocessing catalysts by ultrasonic-assisted leaching with acids. Ind Eng Chem Res. 2011; 50: 9495-9501.
12. Aung HY, Boyarintsev A, Stepanov S, Shoustikov A. Current key options for management of industrial alkaline waste of alumina production (red mud). EDP Sci. 2021; 284: 01003.
13. Turi D, Pusztai J, Nyari I. Causes and circumstances of Red Mud Reservoir Dam failure in 2010 at MAL Zrt Factory Site in Ajka, Hungary. Int. Conf Case Histories in Geotech Eng. Proceeding of 7th Conference of the International Conference on Case Histories in Geotechnical Engineering; 2013 April 29-May 4; Chicago, IL, US. Rolla: Missouri University of Science and Technology. Available from: https://scholarsmine.mst.edu/icchge/7icchge/session03/10.

14. do Carmo FF, Kamino LH, Junior RT, de Campos IC, do Carmo FF, Silvino G, et al. Fundão tailings dam failures: The environment tragedy of the largest technological disaster of Brazilian mining in global context. Perspect Ecol Conserv. 2017; 15: 145-151.
15. Rotta LH, Alcântara E, Park E, Negri RG, Lin YN, Bernardo N, et al. The 2019 Brumadinho tailings dam collapse: Possible cause and impacts of the worst human and environmental disaster in Brazil. Int J Appl Earth Obs Geoinf. 2020; 90: 102119.
16. Greenpeace. Vale's crime in Brumadinho [Internet]. Greenpeace Brasil; 2019. Available from: https://www.greenpeace.org/brasil/o-crime-da-vale-em-brumadinho/.
17. Samal S, Ray AK, Bandopadhyay A. Proposal for resources, utilization and processes of red mud in India—a review. Int J Miner Process. 2013; 118: 43-55.
18. Lima MS, Thives LP. Evaluation of red mud as filler in Brazilian dense graded asphalt mixtures. Constr Build Mater. 2020; 260: 119894.
19. Rychkov V, Botalov M, Kirillov E, Kirillov S, Semenishchev V, Bunkov G, et al. Intensification of carbonate scandium leaching from red mud (bauxite residue). Hydrometallurgy. 2021; 199: 105524.
20. Liu Z, Zong Y, Ma H, Dai W, Li S. Effect of (CaO+ MgO)/SiO_2 ratio on crystallisation and properties of slag glass–ceramics. Adv Appl Ceram. 2014; 113: 411-418.
21. Deihimi N, Irannajad M, Rezai B. Characterization studies of red mud modification processes as adsorbent for enhancing ferricyanide removal. J Environ Manag. 2018; 206: 266-275.
22. Pontikes Y, Nikolopoulos P, Angelopoulos G. Thermal behaviour of clay mixtures with bauxite residue for the production of heavy-clay ceramics. J Eur Ceram Soc. 2007; 27: 1645-1649.
23. Rai S, Wasewar K, Mukhopadhyay J, Yoo CK, Uslu H. Neutralization and utilization of red mud for its better waste management. World. 2012; 6: 5410.
24. Qaidi SM, Tayeh BA, Isleem HF, de Azevedo AR, Ahmed HU, Emad W. Sustainable utilization of red mud waste (bauxite residue) and slag for the production of geopolymer composites: A review. Case Stud Constr Mater. 2022; 16: e00994.
25. Zhang N, Li H, Liu X. Hydration mechanism and leaching behavior of bauxite-calcination-method red mud-coal gangue based cementitious materials. J Hazard Mater. 2016; 314: 172-180.
26. Kurtoğlu SF, Soyer-Uzun S, Uzun A. Tuning structural characteristics of red mud by simple treatments. Ceram Int. 2016; 42: 17581-17593.
27. Liu X, Zhang N, Sun H, Zhang J, Li L. Structural investigation relating to the cementitious activity of bauxite residue—Red mud. Cem Concr Res. 2011; 41: 847-853.
28. Gao Y, Liu Y, Yu H, Zou D. High-entropy oxides for catalysis: Status and perspectives. Appl Catal A. 2022; 631: 118478. doi: 10.1016/j.apcata.2022.118478.
29. Singh K, Guleria H. Strength, durability and micro-structure analysis of self-compacting concrete utilizing industrial by-products. Mod Eng Tech Science. 2020; 2: 1158-1163.
30. Martins M, Silva L, Kuffner B, Barros R, Melo M. Behavior of high strength self-compacting concrete with marble/granite processing waste and waste foundry exhaust sand, subjected to chemical attacks. Constr Build Mater. 2022; 323: 126492.
31. Parashar A, Aggarwal P, Saini B, Aggarwal Y, Bishnoi S. Study on performance enhancement of self-compacting concrete incorporating waste foundry sand. Constr Build Mater. 2020; 251: 118875.
32. Golafshani EM, Behnood A. Predicting the mechanical properties of sustainable concrete containing waste foundry sand using multi-objective ANN approach. Constr Build Mater. 2021;

291: 123314.
33. Mastella MA, Gislon ES, Pelisser F, Ricken C, da Silva L, Angioletto E, et al. Mechanical and toxicological evaluation of concrete artifacts containing waste foundry sand. Waste Manage. 2014; 34: 1495-1500.
34. Dyer PP, de Lima MG. Waste foundry sand in hot mix asphalt: A review. Constr Build Mater. 2022; 359: 129342. doi.org/10.1016/j.conbuildmat.2022.129342
35. Yaghoubi E, Arulrajah A, Yaghoubi M, Horpibulsuk S. Shear strength properties and stress–strain behavior of waste foundry sand. Constr Build Mater. 2020; 249: 118761.
36. Mymrin V, Ribeiro RA, Alekseev K, Zelinskaya E, Tolmacheva N, Catai R. Environment friendly ceramics from hazardous industrial wastes. Ceram Int. 2014; 40: 9427-9437.
37. Coppio GJ, de Lima MG, Lencioni JW, Cividanes LS, Dyer PP, Silva SA. Surface electrical resistivity and compressive strength of concrete with the use of waste foundry sand as aggregate. Constr Build Mater. 2019; 212: 514-521.
38. Damayanti R, Khareunissa H. Composition and characteristics of red mud: A case study on tayan bauxite residue from alumina processing plant at west kalimantan. Indones Min J. 2016; 19: 179-190.
39. Oliveira GE, Holanda JNF. Use of mix of clay/solid waste from steel works for civil construction materials. Waste Manag Res. 2004; 22: 358-363.
40. Wendling L, Douglas G, Coleman S. Characterisation of mining and industrial by-products with potential for use as environmental amendments. Water for a healthy country national research flagship report; 2009.
41. NBR 7170: Solid ceramic brick for masonry - Specification. Brazilian Association of Technical Standards. Rio de Janeiro; 2012.
42. NBR 10.004 Solid waste – Classification. Brazilian Association of Technical Standards. Rio de Janeiro; 2004.